CHAPTER 3

Schottky barrier Ultraviolet Photodetectors

3.1 Introduction

The theoretical background of Schottky barrier photodiodes is given in this chapter. Firstly a discussion of the fundamental operation and evaluation of photodiodes is discussed in section 3.2. Section 3.3 discusses the theory of Schottky barrier junctions. The transport mechanisms of Schottky contacts are discussed in section 3.4. This chapter finishes with the applications of Schottky barriers to the photodiodes.

3.2 Ultraviolet (UV) photodetectors

Semiconductor photodiodes work in three fundamental modes:

- Photoconductive detectors
- p-n junction photodiodes
- Schottky barrier diodes.

These are miniature in size, lightweight, and are easily integrated into microelectronic systems. They are very fast and responsive, with relatively little noise. These devices shows high quantum efficiency and low leakage currents; are insensitive to magnetic fields, superior to glass vacuum devices in reliability and have average ability to store charge and integrate detected signal [1]. They can be used in reverse bias mode of photoconductive detector operation or zero bias modes of photovoltaic detector operation and have linear photo-current flux characteristics. The current-voltage (I-V) characteristic of a photodiode follows the standard diode equation [2]:

$$I = I_s \left(\exp[\frac{qV}{kT} - 1] \right) \tag{3.1}$$

where I_s is the saturation current V is the applied voltage q is the electronic charge, T is the temperature, k is Botlzman constant. When a photodiode is illuminated with electromagnetic

radiation, equation 3.1 is modified due to the generation of additional carriers within the device and it becomes [3]:

$$I = I_s \left(\exp\left[\frac{qV}{kT} - 1 \right] \right) - qAG\ L_p + L_n \tag{3.2}$$

where A is the device area, G is the carrier generation rate; L_p and L_n are diffusion lengths for holes and electrons respectively. When incident electromagnetic radiation is greater than the bandgap of the semiconductor, some of the radiation will be absorbed, creating electron-hole pairs, due to photon-electron scattering. As the photons are absorbed by the semiconductor, they interact with electrons in the valence band, giving them enough energy to be promoted to the conduction band. A hole is left in the valence band, and we have generated an electron hole pair in the semiconductor, which follows the carrier drift process, as shown in figure 3.1.
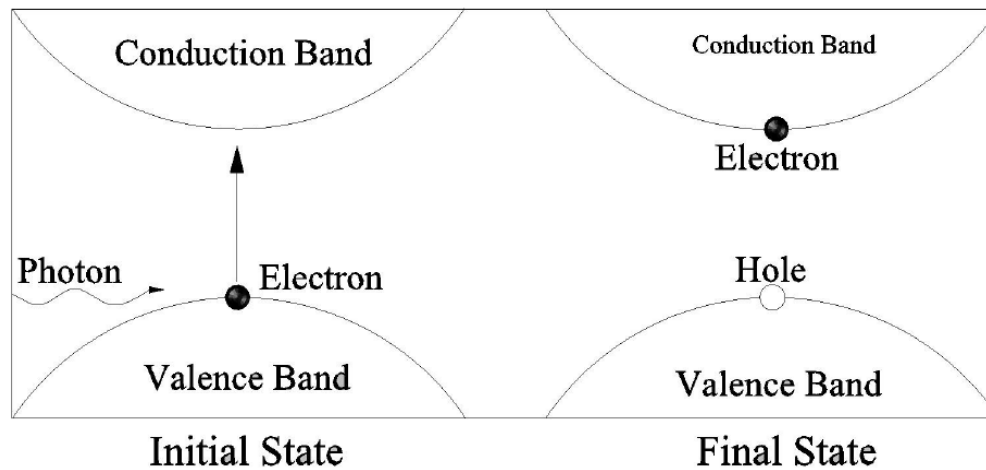

Figure 3.1: Schematics of photon absorption in a direct bandgap semiconductor

The electrons are then swept out by the built-in voltage in the depletion region into the n-type side and holes go to the p-type side of the device. If the absorption occurs within L_n of the depletion region on the p-side of the junction, the electrons may diffuse into the space charge region before recombining and swept out into the n-type region. Similar process occurs for holes

within the L_p of the depletion region. This implies that the total photocurrent is contributed by both the carrier diffusion and drift. The depletion region of the device makes a significant contribution to the device detection efficiency. Some of the parameters of semiconductor photodiodes, which are used in detection mechanisms follows:

3.2.1   Active area of semiconductor diode (A)

The design of photodiodes requires that the device have an area, through which incident radiation can be freely absorbed, called active area, as shown in figure 3.2 [4]. This is accomplished by providing a window between the ohmic and Schottky contact for nitride based semiconductors, ranging from 0.1 to 100 mm [5-6]. The thickness of the metal for Schottky contacts is made sufficiently thin so that it is transparent to incident UV radiation, to optimize photon absorption.
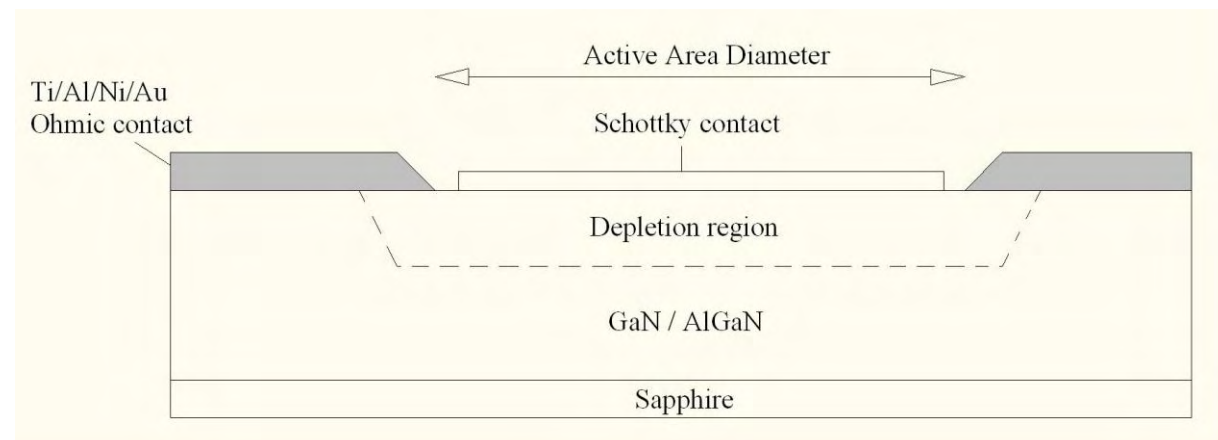

Figure 3.2: Schematics of AlGaN/GaN Schottky barrier photodiode, showing active area.

3.2.2 Responsivity

Responsivity, R_λ of the device is defined as the ratio of the photocurrent I_p to the incident electromagnetic radiation power, *(P)* given by [7]:

$$R_\lambda = \frac{I_p}{P} \tag{3.3}$$

The quantum efficiency is the average number of electron-hole-pairs generated by each incident photon, defined as the fraction of incident photons that contribute to photocurrent, and it is related to responsivity by:

$$Q.E = \frac{R_{\lambda \; observed}}{R_{\lambda \; ideal}} = R_{\lambda} \frac{hc}{\lambda q} = 1240 \frac{R_{\lambda}}{\lambda} \qquad (3.4)$$

where h is Planck's constant, c is the speed of light and λ is the wavelength of incident radiation. Another parameter, related to responsivity is the $R_0 A$ product, where R_0 is the dynamic resistance of the diode at zero bias and A is the diode area. A large $R_0 A$ product is necessary for the detector to have large detectivity, D^* meaning that it is able to produce a measurable signal current at very low radiation level. If the detector is limited by thermal noise, then detectivity becomes:

$$D^* = \frac{q\eta}{h\nu}\left(\frac{R_0 A}{4kT}\right)^{\frac{1}{2}} \qquad (3.5)$$

where η is the quantum efficiency. The detectivity may also be expressed in terms of noise equivalent power (NEP). The NEP is a quantity that signifies the root means square (rms) optical power of an output signal required to generate the noise level present in the detector over a bandwidth of 1 Hz. The detectivity is then expressed as:

$$D^* = \frac{\sqrt{A\Delta f}}{NEP} \qquad (3.6)$$

where Δf is the detector bandwidth and f is the noise frequency. Consequently current responsivity may be written as:

$$R_i = \frac{q\lambda}{hc}\eta \qquad (3.7)$$

and the voltage responsivity:

$$R_V = \frac{q\lambda}{hc}\eta R \tag{3.8}$$

where $R = (dI/dV)^{-1}$ is the differential resistance of the photodiode.

3.2.3 Operation voltage V_{op}

Metal-semiconductor photodiodes can be used in zero and reverse bias modes of photovoltaic operation, with the operation voltage lower than the breakdown voltage, V_{BR}. This is the maximum reverse voltage that can be safely applied to the photodiode before a breakdown at the junction occurs. The V_{BR} for abrupt p-n junctions and Schottky barriers is given by:

$$V_{BR} = 60\left(\frac{E_g}{1.1}\right)^{3/2}\left(\frac{N_i}{10^{16}}\right)^{-3/4} \tag{3.9}$$

where E_g is the bandgap, N_i is the carrier density (cm^{-3}). If the external reverse bias is increased, the applied voltage increases, thereby increasing the size of the depletion region within the device [8].

3.2.4 Dark Current-Voltage characteristics ($I_d - V_d$)

$I-V$ characteristics of Schottky barrier photodiodes exhibiting a thermionic emission mechanism of current flow is:

$$I_d = I_s\left[\exp\left(\frac{qV_d}{nkT}\right) - 1\right] = A^*AT^2\exp\left(-\frac{q\varphi_B}{kT}\right)\left[\exp\left(\frac{qV_d}{nkT}\right) - 1\right] \tag{3.10}$$

where I_s is the saturation current, n is the ideality factor, A is the area, V_d is the applied voltage and A^* is the Richardson constant and φ_B is the barrier height. These variables are used in the calculation of the shunt resistance of a photodiode. $R_0 = nkT/qI_s$ is dark resistance and I_d is

dark current at the operation voltage. High temperature annealing is known to reduce the leakage and dark current in a Schottky contact [9].

3.2.5 Response speed

The response speed of a photodiode determines its ability to follow a fast-varying optical signal. For the optical signal to be acceptable, a photodiode must have a speed higher than frequency response. The speed of a photodiode is related to the response time by rise-time, t_r, or fall-time, t_f, of its response to an impulse signal. The rise-time is defined as the time interval for the response to increase from 10% to 90% of its of peak value, and the fall-time is from 90% to 10% of its decay value [10]. The equation for the response speed is then given by:

$$\varsigma \frac{90}{10} = \left[\varsigma_{cc}^2 + \varsigma_{Diff}^2 + \varsigma_{RC}^2 \right]^{1/2} \tag{3.11}$$

where ς_{cc} is the time for charge collection from the depleted region, ς_{Diff} the time for photo-generated carriers to diffuse to the depleted region and ς_{RC} is the time constant. We further define ς_{cc} as:

$$\varsigma_{cc} = \frac{W_d}{2v_d} \tag{3.12}$$

where W_d is the width of the depletion region and v_d is the drift velocity of the photo-generated carriers. ς_{Diff} is defined as:

$$\varsigma_{Diff} = \left(\frac{W_0 - W_d}{D_p} \right)^2 \tag{3.13}$$

where W_0 is the thickness of the substrate and D_p is the diffusion constant. Finally, ς_{RC} is given by:

$$\varsigma_{RC} = 2.2 \left(R_s + R_L \right) C_V \tag{3.14}$$

where R_s is the series resistance of the photodiode and C_V is the capacitance at applied voltage V. When a reverse bias is applied to the depletion region, the width thereof increases and collection time for the photo-generated carriers becomes larger.

3.2.6 Capacitance (C)

Junction capacitance is the ability of the photodiode to store charge. This value depends on the substrate resistivity, the reverse bias voltage and the active area. In the case of Schottky barriers, C is given by:

$$C = A \left[\frac{\varepsilon_s \varepsilon_0 q N_i}{2 \left(V_{bi} + V_d - kT/q \right)} \right]^{1/2} \tag{3.15}$$

where ε_s and ε_0 are the dielectric constants of semiconductor and vacuum respectively, V_{bi} and V_d are built-in and applied voltages. Capacitance is an important parameter that determines the response speed of the photodiode by relating the depletion with mobility of majority carriers and resistivity of the semiconductor. The zero-biased photodiode gives capacitance that is inversely proportional to the substrate resistivity. High resistivity materials yield small capacitance [11].

3.2.7 Series Resistance R_s

Series resistance R_s is the resistance of a detector through which the photodiode current must flow and is the sum of resistances of semiconductor bulk and ohmic contacts. The general expression for series resistance is given by:

$$R_s = \frac{(W_0 - W_d)\rho}{A} + R_c \tag{3.16}$$

The first term is the series resistance of the quasi-neutral region with W_0 and W_d being the thicknesses of the substrate and the depletion region respectively and A is the diode area. R_c is the resistance due to ohmic contact and the semiconductor. Series resistance decreases linearly with increasing carrier concentration.

3.3 Modifications to Schottky-Mott Theory

According to Schottky-Mott theory [12,13] the rectifying property of the metal-semiconductor junction arises from the presence of a barrier between the metal and the semiconductor, resulting from the difference in the work functions, φ_m and φ_s of the metal and the semiconductor [14]. In order for the contact to be rectifying, it is required that $\varphi_m > \varphi_s$ for n-type semiconductor. The barrier heights for n- and p-type semiconductors are given by [11]:

$$
\begin{aligned}
\varphi_{bn} &= \varphi_m - \chi_s \\
\varphi_{bp} &= \chi_s + E_g - \varphi_m
\end{aligned}
\tag{3.17}
$$

where χ_s is the electron affinity of the semiconductor and E_g is the semiconductor bandgap. Figure 3.3 shows the energy band diagrams of Schottky barrier for n- and p-type semiconductors. The potential barrier, caused by band bending between the bulk of the semiconductor and the metal-semiconductor interface, is given by:

$$
\psi_s = \varphi_m - \varphi_s
\tag{3.18}
$$

where ψ_s is the barrier potential. In practice, however, the built-in potential barrier does not follow such a simple relationship with φ_m, and is effectively reduced as a result of the interface states originating from either surface states or metal-induced gap (MIG) states and to interfacial reactions at the junction. Published results show considerable variations among experimental data on the values of the metal work function, φ_m [15]. Their analysis indicates an empirical relationship of the form [16, 17].

$$\varphi_b = \Upsilon_1 \varphi_m + \Upsilon_2 \tag{3.19}$$

where Υ_1 and Υ_2 are constants characteristics of the semiconductor. The limits, $\Upsilon_1 = 0$ and $\Upsilon_1 = 1$ indicates that the barrier is due to localized surface states and the ideal Schottky barrier, respectively. The contribution of the surface states to barrier height has been discussed by Bardeen [18]. The slope parameter $\Upsilon_1 = \partial \varphi_b / \partial \varphi_m$ can be used to describe the extent of Fermi level pinning for a given semiconductor. The parameters Υ_1 and Υ_2 have been used by some researchers to estimate the interface states density [16].

Cowley and Sze [19] have shown that, according to Bardeen model, the barrier height, in the case of n-type semiconductor is approximately given by:

$$\varphi_{on} = \Upsilon \left(\varphi_m - \chi_s \right) + \left(1 - \Upsilon \right) \left(E_g - \varphi_0 \right) - \Delta \varphi \tag{3.20}$$

where $\Upsilon = \varepsilon_i / \left(\varepsilon_i + q \delta D_g \right)$ and φ_0 term is the position of the neutral level of the interface states measured from the top of the valence band, $\Delta \varphi$ is the barrier lowering as a result of the image forces, δ is the thickness of the interfacial layer and ε_i is its total permittivity. The surface states are assumed to be uniformly distributed in energy within the bandgap, with density D_g per electron volt per unit area. For very high density of states, Υ becomes very small and φ_{bn} approaches the value $E_g - \varphi_0$. This is because a very small deviation of the Fermi level from the neutral level can produce a large dipole moment, which stabilizes the barrier height. The Fermi level is stabilized or pinned relative to the band edges by the surface states.
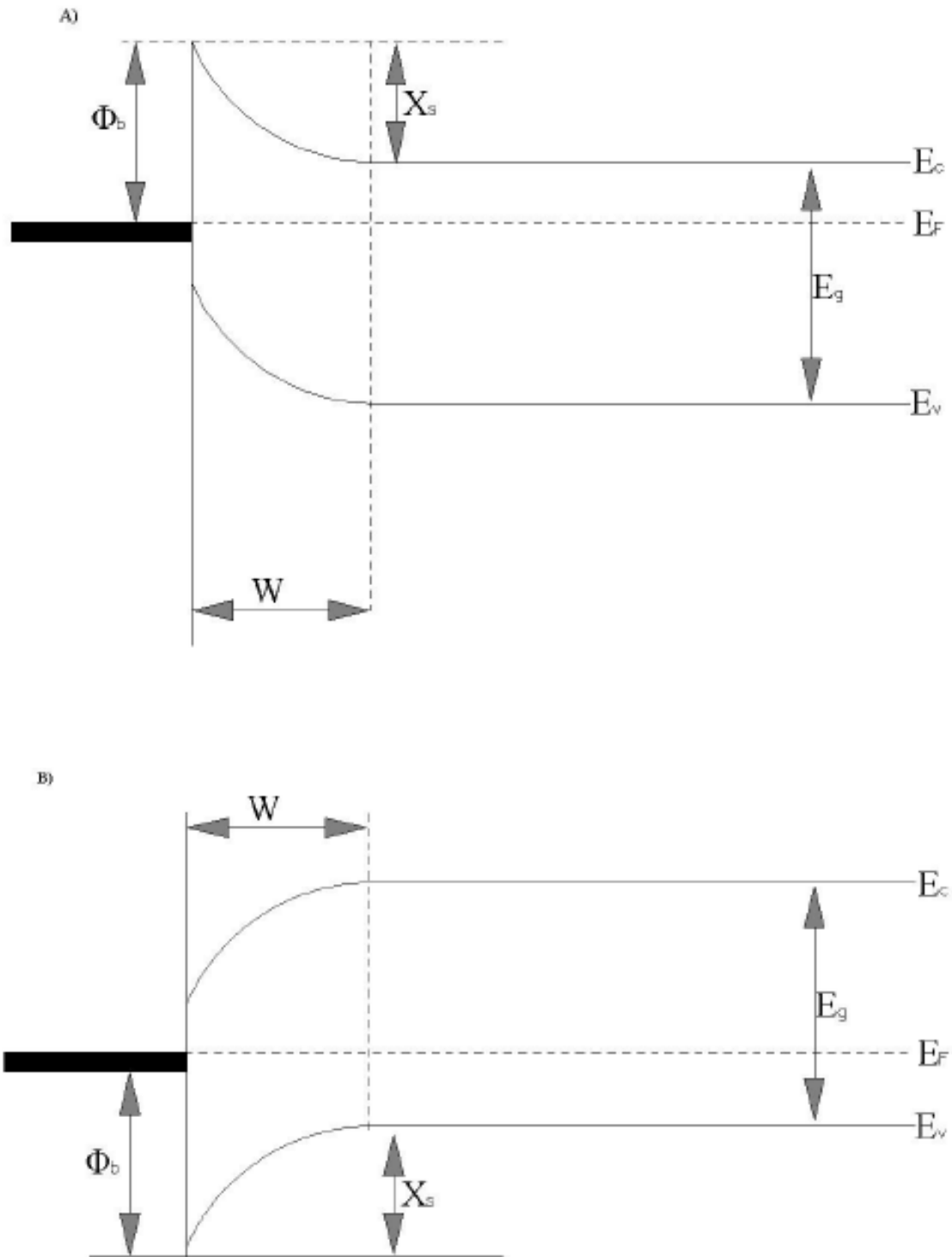
A)

Φ_b

X_s

E_c

E_F

E_g

E_v

W

B)

W

E_c

E_g

E_F

E_v

Φ_b

X_s

Figure 3.3: Energy band diagrams of Schottky barrier for (A) n- and (B) p-type semiconductors.

3.4   Charge Transport Mechanisms.

The charge transport mechanisms in Schottky barrier diodes, as shown in figure 3.4, are mainly due to majority carriers, the electrons, across the metal-semiconductor junction. These mechanisms are classified as:

A. The emission of electrons from the semiconductor over the top of the potential barrier into the metal,

B. Quantum-mechanical tunneling of electrons through the barrier,

C. Recombination in space-charge region and

D. Recombination in the neutral region (equivalent to hole injection from metal to semiconductor).
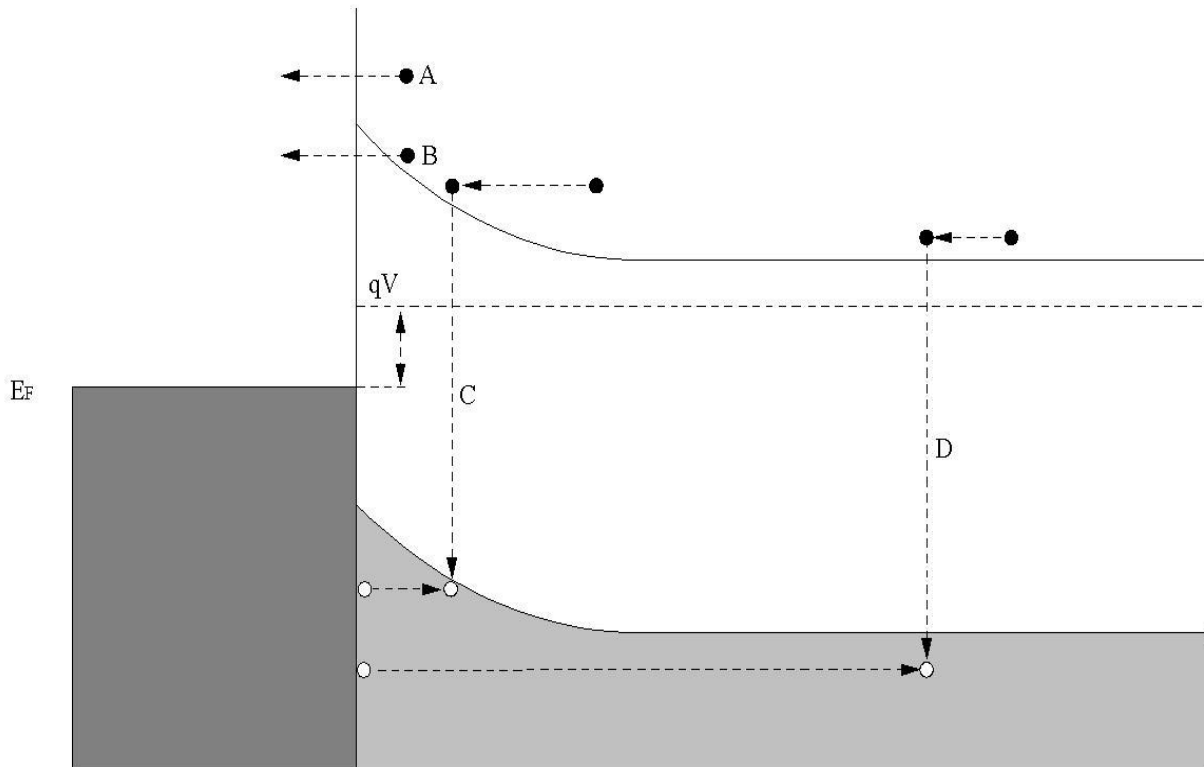

Figure 3.4: Energy band diagram of a forward biased Schottky contact on n-type semiconductor showing different charge transport processes [14]

There may also be edge leakage current due to high electric field at the contact periphery or interface current due to traps at the metal-semiconductor interface. The inverse processes occur under reverse bias. The transports of electrons over the potential barrier have been described by various theories:

- diffusion theory of Schottky and Spenke [20,21],
- Bethe's thermionic emission [22]
- and unified thermionic emission diffusion.

It is now generally accepted that, for high-mobility semiconductors with acceptable impurity concentrations, the thermionic emission theory appears to qualitatively explains the experimentally observed current-voltage ($I-V$) characteristics [23]. Some researchers [24] have also included in the simple thermionic emission theory the effect of quantum-mechanical reflection and tunneling of carriers through the barrier; and have tried to obtain modified analytical expression for ($I-V$) characteristics. Consequently, this has led to a lowering of the barrier height and a rounding off at the top, known as the Schottky effect. The rounding off at the top is the image force lowering of the potential energy for charge carriers' emission due to an applied electric field. Bethe's thermionic emission theory is derived from the following assumptions:

- the barrier height is far larger than kT,
- thermal equilibrium is established at the plane that determines emission,
- and the existence of a net current does not affect this equilibrium.

The barrier height is then extracted from the slope of the linear line resulting from the logarithmic plot of current – voltage ($I-V$) across the Schottky diode. The criterion used by Bethe for the $I-V$ slope of the barrier is that it must decrease by more than kT over a distance equal to the scattering length. The resulting charge flow will depend only on the barrier height, The saturation current is independent of the applied bias.

3.5 Theory of Schottky Barrier ultraviolet photodiodes

The photosensitivity of Schottky barrier diodes is determined by the following:

- Firstly, electrons are generated in the metal and they are injected into the semiconductor at incident photon energies exceeding the height $q\varphi_b$ of the metal-semiconductor potential barrier. When $q\varphi_b < h\nu < E_g$ the short-circuit current I_{p0} varies with the photon energy according to Fowler law [25,26].

$$I_{p0} \sim \left(h\nu - q\varphi_b \right)^2 \tag{3.21}$$

- Secondly, electron-hole pairs are generated in the semiconductor, then separated by built in electric field at $h\nu > E_g$. Then, the photocurrent is the sum of the contributions from the charge carriers generated in the space-charge layer of width W and the carriers that reached the layer from the adjoining region of extent L (minority charge diffusion length), given by [27]:

$$I_{p0} = -q\eta \left(1 - R \right) \Phi \left(\frac{1 - \exp(\alpha W)}{1 + \alpha L} \right) \tag{3.22}$$

where α is the semiconductor light absorption coefficient and Φ the incident flux.

The energy-band diagrams of a Schottky barrier photodetector are shown in figure 3.5.
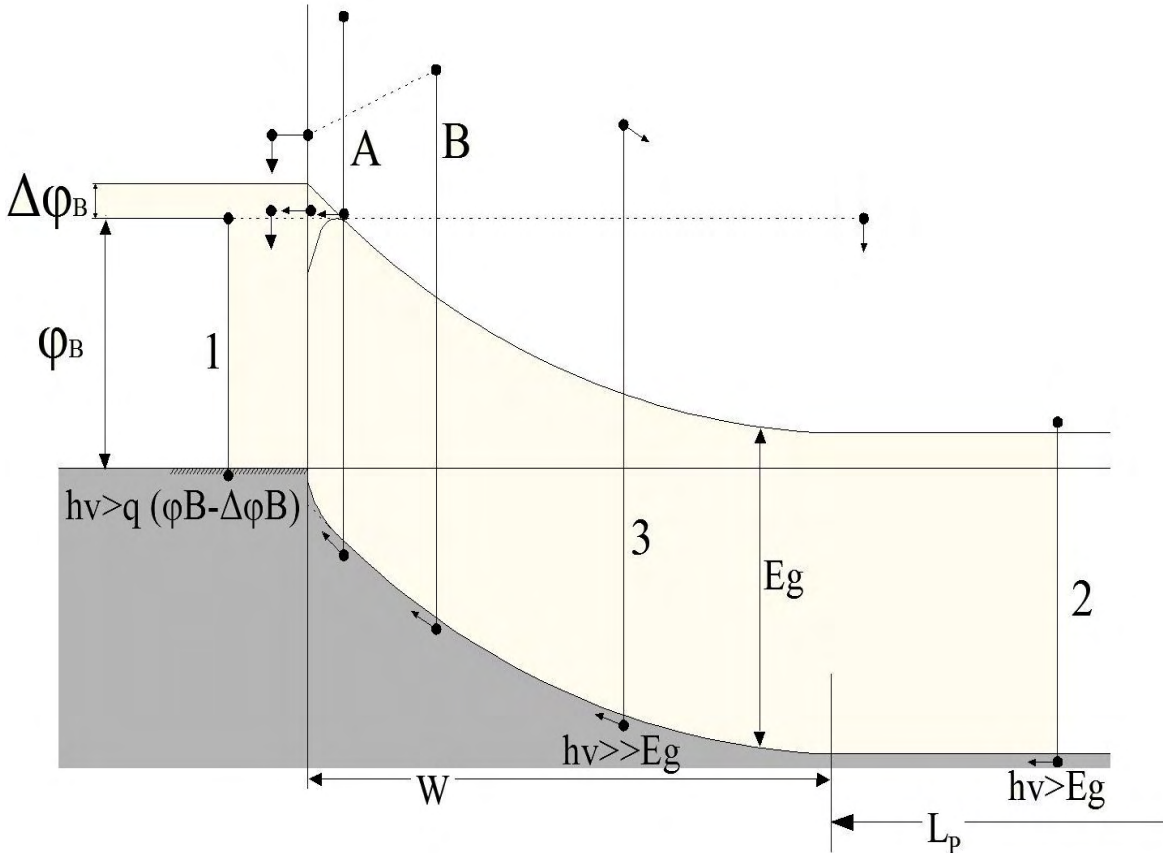
Figure 3.5: Energy band diagrams of a Schottky barrier photodetector

Comparing these mechanisms, the second process is more efficient than the first and therefore the long wavelength limit of the photosensitivity spectrum is close to the bandgap value in direct-band semiconductors and to the threshold energy for direct optical transitions in the indirect bandgap semiconductors. At photon energies far above the bandgap, the photosensitivity is observed to drop, and explained by loss of carriers generated by photons through carrier drift against the built in electric field [28], by thermionic emission, by quasiballistic electron transport or by a drop in internal quantum yield [29].

REFERENCES

[1]   Goldberg Y. A., Semiconductor Sciience and Technology **14** (1999) R41.

[2]   Schockley W.. Bell Systems Journal **28** (1949) 435.

[3]   Streetman B. and Banerjee S., Solid State Electronics, Prentice Hall, New York (2000).

[4]   Jiang H. and Egawa T., Electronic Letters **42** (19) (2006) 884.

[5]   Collins C.J, Chowdhury U., Wong M. M., Yang B., Beck A. L., Dupuis R. D. and Campbell J. C., Electronic Letters **38** (2002) 824.

[6]   Asalm S. .Vest R. E., Franz D., Yan F. and Zhao Y., Electronic Letters **40** (2005) 1080.

[7]   Dereniak E. L. and Growe D. G., Optical Radiation Detectors, Wiley, New York (1984).

[8]   Sze S. M., Physics of Semiconductors, 2nd Edition, Wiley, New York (1981).

[9]   Lee Y. C., Hassan Z., Abdullah M. J., Hashim M. R., and Ibrahim K., Microelectronic Engineering **81** (2005) 262.

[10]   Graeme J., Photodiode Amplifiers, McGraw Hill, New York, (1996).

[11]   Tyagi M. S., in Metal-Semiconductor Schottky Barrier Junctions and their applications, edited by B. L. Sharma, New York, (1984).

[12]   Schottky W. S., Naturwissenschaften **26** (1938) 843.

[13]   Mott N. F., Proceedings Cambridge Philosophical Society **34** (1938) 568.

[14]   Rhoderick E. H., Metal-Semiconductor Contacts, Oxford, Clarendon, (1978).

[15]   Rhoderick E. H., IEEE Proceedings **129** (1982) 1.

[16]   Johnson E. O., RCA Review. **26** (1965) 163.

[17]   Razeghi M. and Rogalski A. Semiconductor Ultraviolet Photodetectors Journal of Applied Physysics **79** (1996) 7433.

[18]   Bardeen J., Physical Reveview **71** (1947) 717.

[19]   Cowley A. M. and Sze S. M., Journal Applied Physics **36** (1965) 3212.

[20]   Schottky W. and Spenke E., Wiss. Veroff. Siemens-Werken. **18** (1939) 225.

[21]   Spenke E., Electronic Semiconductors, McGraw-Hill, New York, (1958).

[22]   Bethe H. A., MIT Radiation Laboratory Report **43-12** (1942).

[23]   Crowell C. R. and Sze S. M., Solid State Electronics **9** (1966) 1035.

[24]   Ottaviani G., Tu K. N. and Mayer J. W., Physical Review Letters **44** (1980) 284.

[25]   Fowler R. H., Physical Review **38** (1931) 45.

[26]   Anderson C. L., Crowell C. R., and Kao T. W., Solid State Electronics **18** (1975) 705.

[27]   Gartner W. W. Physical Review **116** (1959) 84.

[28]   Li SS, Lindholm F. A., and Wang C. T., Journal of Applied Physics **43** (1972) 4123.

[29]   Goldberg Y. A, Konstantinov O. V., Posse E. A. and Tsarenkov B. V., Semiconductors **29** (1995) 215.

CHAPTER 4

Experimental Techniques

4.1 Introduction

In this chapter, the experimental techniques used in the study are discussed. The performance of Schottky barrier diodes depends on processing issues such as cleaning, the etching of the surface and low surface roughness. Different wet chemicals have been used to reach a stoichiometric GaN surface, characterizing the surface with Auger Electron Spectroscopy (AES) and X-ray Photoelectron Spectroscopy (XPS). The surface topography and roughness were evaluated using a Scanning Electron Microscope (SEM) and an Atomic Force Microscope (AFM). Schottky diodes were fabricated by depositing a metal layer onto the semiconductor using an electron beam and resistive evaporator, depending on the density of the metal. The metals were chosen according to the percentage of UV light transmitted through layers of different thicknesses. The metal was selected with the aid of an in-house computer program

4.2 Sample preparation

n-GaN samples were grown by MOCVD from AIXTRON and HVPE from TDI. As grown samples were degreased in boiling trichloroethylene and isopropanol. HCl:HNO$_3$ aquaregia was used to remove metal particles and a final rinse in dilute HCl. Each cleaning step was followed by rinsing in deionized water. After cleaning, samples were loaded in AES to evaluate the surface elements and stoichiometry. Morphological studied were done in the SEM and AFM. The samples were then loaded in the electron beam deposition and ohmic contacts were deposited. The contacts were then annealed in the vacuum furnace at 500 °C. Samples were further etched in dilute HCl and then Schottky contacts were deposited. The diodes were then ready for electrical and optical characterization techniques.

4.3 Surface Characterization

4.3.1 Auger Electron Spectroscopy

AES [1] is a suitable technique for surface analysis because it is capable of identifying individual elements. It is a very sensitive surface technique which can measure to a depth of 1 - 3 nm. It can also be used to obtain depth profiling measurements for determining the concentration of surface species. Auger electrons are produced in the ionization process of an atom hit by primary electrons. The process continues with an electron from the higher energy level being attracted to the ionized atom to take it back to a stable state. Auger electrons are then produced from the excess energy resulting from stabilization, which may be absorbed by the sample or detected on the outer monolayers of the surface. The specific energy involved in the transition process is the key to the identification of the elements that produced the Auger electrons. Figure 4.1 shows a picture of the AES. AES has the ability to remove the surface contaminants with the electron beam, in a process called desorption. In this work, it was observed that Cl on the GaN surface was desorbed to the lowest detection limit of the AES during continuous exposure of the surface to the electron beam. The addition of a heater block inside the ultra-high vacuum AES removes surface contaminants, such as those common to the semiconductors, namely O and C. Other elements introduced onto the GaN surface from the chemicals used in the wet cleaning and etching are reduced by exposure to the electron beam and thermal heating inside the AES.
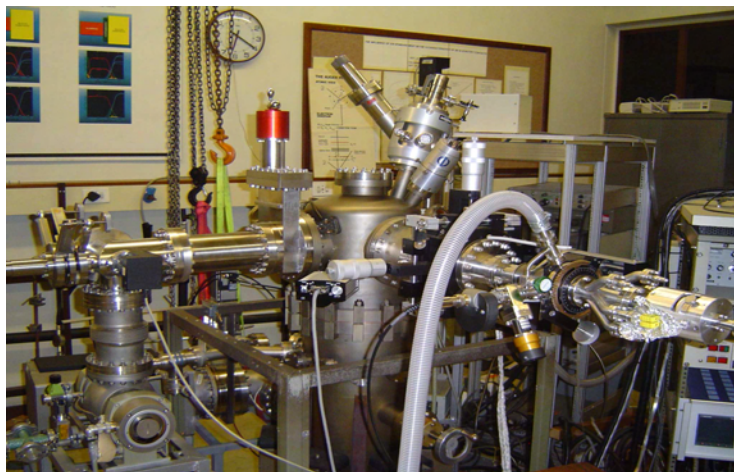

Figure 4.1: Pictorial presentation of the AES at the University of Pretoria.

4.3.2   Scanning Electron Spectroscopy

SEM, as shown in figure 4.2, [2] is a high resolution surface technique suitable for imaging surface defects on conducting materials. It creates a highly focused electron beam which scans in a regular manner over the sample, while the detector measures the resulting scattered electrons. When focused on the surface, the electron beam stimulates the emission of secondary electrons, which are amplified to increase the brightness of the Cathode Ray Tube (CRT) display. A point by point communication exists between the brightness of each point in the CRT and the number of electrons emitted from the sample surface. The energy of the electrons is directly related to the desired image. A high energy electron beam (5 – 50 keV) is used to identify deep structures while making it possible to produce nondestructive images below the surface, up to 20 µm. A useful component of the SEM is the Energy Dispersive X-ray Spectrometer (EDAX) which is characteristic of X-rays produced by primary electrons emitted from the sample, used to identify the elemental species on the surface. The typical pressure of the SEM was about 10^{-6} torr.
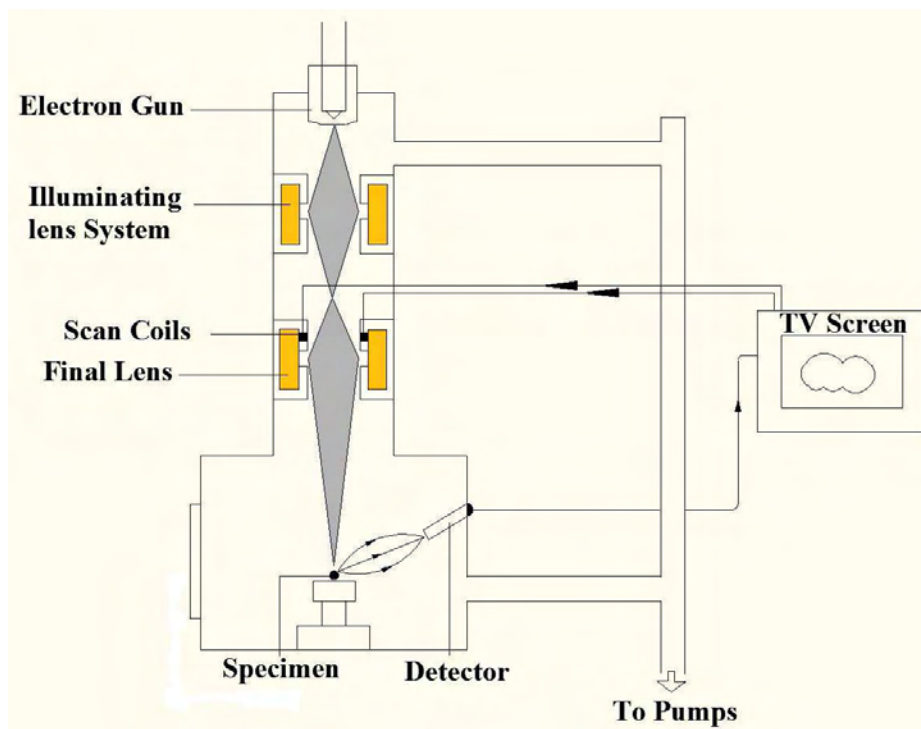

Figure 4.2: Schematics of the SEM operation

4.3.3 Atomic Force Microscopy

AFM [3] is capable of producing three dimensional views of the surface morphology. The advantage of using the AFM is the resolution of the atomic image and ability to measure the force on the nanoscale. The AFM consists of a tip at the end of a flexible cantilever across the sample surface while maintaining a small constant force. Figure 4.3 depicts the schematics of the AFM. The laser, focused on the cantilever, senses the position of the tip relative to the surface, detecting the topography. The laser beam is deflected into a dual element sensor during the scanning. The sensor measures the difference in light intensities registered at the detectors, converting the signals into voltage. The relevant software captures the voltage signals and converts them into an image of the surface. The piezoelectric drive unit monitors the difference in the height sensed from the surface. There are different modes of operating the AFM; the most common is the contact mode where the tip scans the surface in close contact with the surface of the sample. The constant force of about 10^{-9} N at the tip is repulsive, pushing the cantilever against the sample surface with the piezoelectric unit. In this work, the AFM was used in contact mode, employing scanners of 100 X 100 and 7 X 7 µm. The reliability of the results relies on the position of the AFM unit: it should be placed on a stable table.
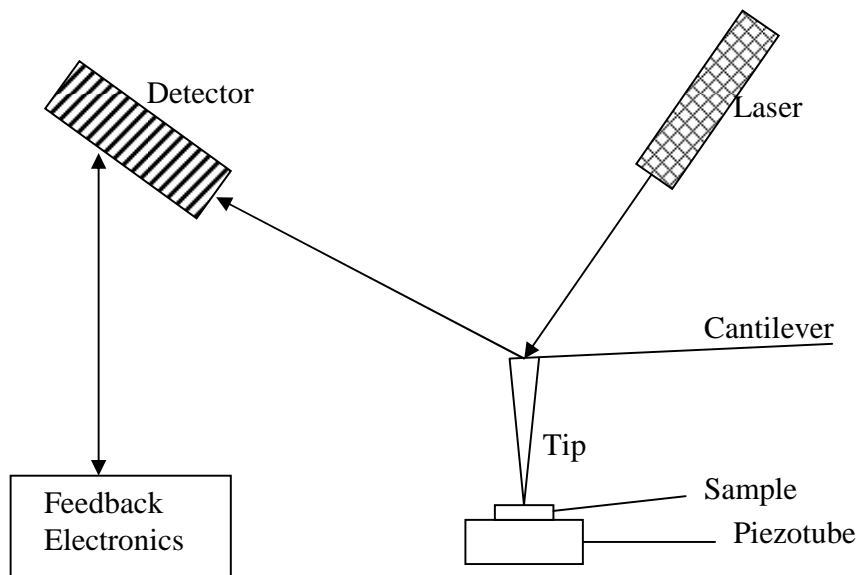

Figure 4.3: Schematics of the AFM operation

4.4 Electrical and Optical Characterization

Current-Voltage *(I-V)* measurements are used to evaluate the rectifying properties of the Schottky barrier diodes (SBD) [4]. The parameters of interest in these measurements are the series resistance (R_s), Schottky barrier height (ϕ_B), saturation current measured at 1 V (I_0) and ideality factor (*n*). Figure 4.4 illustrates the *I-V* characteristics of an ideal and practical SBD. For an ideal Schottky diode, $n = 1$, while practically it is above unity, depending on transport mechanisms. In determining the *I-V* parameters, it is assumed that the current transport is dominated by thermionic emission. The barrier height is then extracted by fitting a straight line in region (b) of the *I-V* plot in figure 4.4. From equation 3.10, the y-intercept of the fit gives the saturation current $I_s = AA^{**}T^2.\exp[-q\varphi_{bo}/kT]$ thus the barrier height is given by $\varphi_{b0} = kT/q \ln\left(AA^{**}T^2/I_0\right)$, where A is the diode area, T is the measurements temperature, k is the Boltzmann constant, q is the electronic charge and the modified Richardson plot, A^{**}. This approach requires the knowledge of the modified Richardson plot, A^{**} for a Schottky contact. The more accurate value of the barrier height is extracted using the Arrhenius plot [$\ln\left(I/T^2\right)$ - $1/T$]. The Ideality factor is then extracted from the linear fit of the same region and is expressed as $n = (q/kT).\left(V_a/\ln[I/I_0]\right)$. The series resistance is determined form region (c) of figure 4.4, where the voltage is high. The plot assumes a flat state and R_s is extracted from the I-V plot. The leakage current is defined as the current flowing when an ideal current is zero. In particular, leakage occurs when electrons or holes tunnel through an insulator and increases exponentially as the insulating region becomes small [5]. In the case of a Schottky contact, tunneling of carriers occurs between the metal and the semiconductor at the interface. It is of vital importance to measure leakage currents in diodes as they lead to device failure when too high. Figure 4.4 (d) shows the reverse leakage current of a practical diode, and compared with the ideal case, it has to be almost constant and as low as possible.
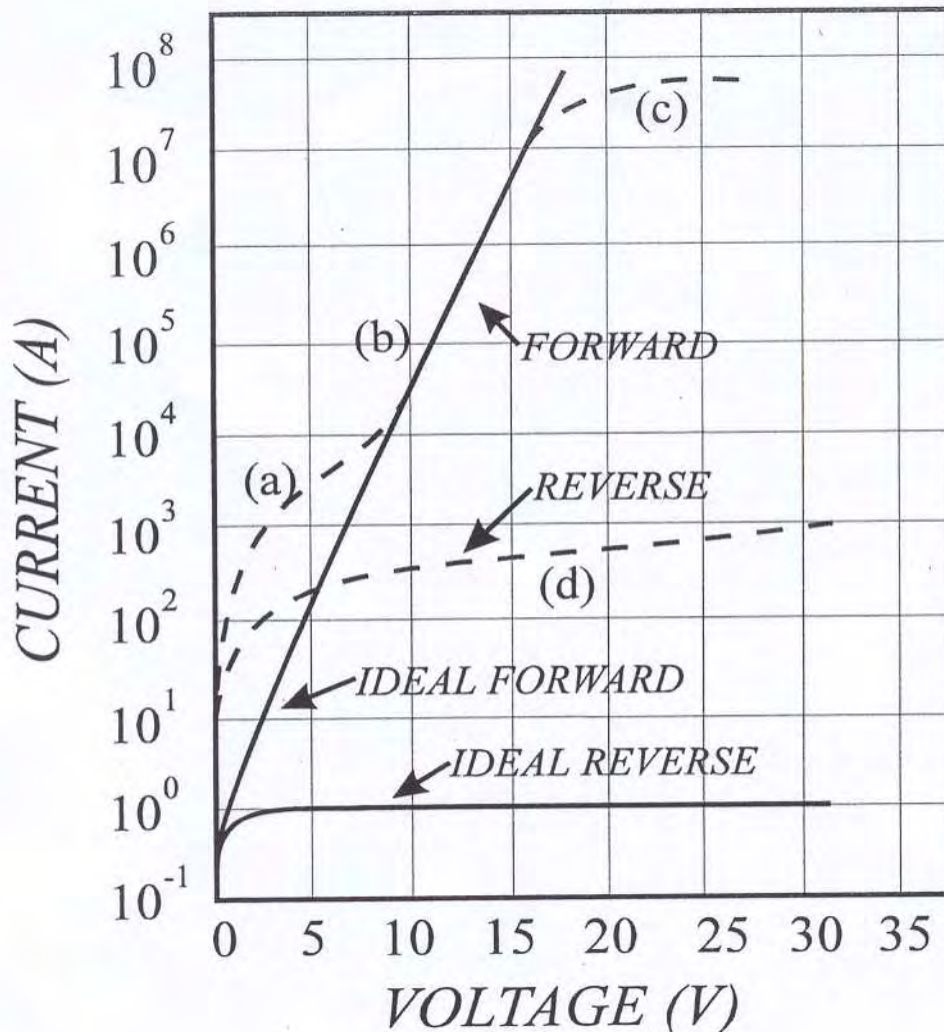
Figure 4.4: Current-Voltage characteristics of an ideal and a practical Schottky barrier diode: (a) generation-recombination current region; (b) diffusion current region; (c) series resistance effect; (d) reverse leakage current due to generation-recombination and surface effects [adapted from [7].

The capacitance-voltage (*C-V*) measurements also offer another method for evaluation of the barrier height including the built-in potential (V_{bi}) and the carrier density, N_D. When a metal and a semiconductor come into intimate contact, the conduction and valence bands of the material are lined with the Fermi level at equilibrium. This relationship gives the boundary conditions for the Poisson equation, where the depletion width (*W*) of a reverse biased Schottky contact is given

by $W = \sqrt{2\varepsilon_s / qN_D \left(V_{bi} - V_a - kT/q \right)}$, where ε_s is the permittivity and V_a is the applied voltage. The space charge per unit area is given by $Q_{sc} = qN_d W$ and the depletion region capacitance per unit area at the contact is approximated to that of a parallel plate capacitor given by $C = \varepsilon_s / W$ and can be rewritten as $1/C^2 = 2((V_{bi} - Va - kT/q)/q\varepsilon_s N_D$, and the data from *C-V* measurements can be used to plot $1/C^2$ as a function of applied voltage, where the x-axis intercept yield the built-in potential, V_{bi}. The carrier density can be obtained from $N_D = 2/q\varepsilon_s \left[-1/d/dV \left(1/C^2 \right) \right]$. The *C-V* barrier height is obtained from $\varphi_b = V_i + V_n + kT/q - \Delta\varphi$ [6]. Furthermore, the measurements can be used to study the impurity levels in semiconductors.

The optical characterization of the individual diodes is created using a UV light with a monochromator source to select wavelengths. The use of monochromated light makes the measurement of photo-generated current as a function of wavelength and voltage possible. The photocurrent is then used to compute the responsivity, quantum efficiency, detectivity and noise equivalent power of the photodiodes. The responsivity is calculated from equation 3.3. The responsivity value is then used in equation 3.4 to calculate the quantum efficiency. The set-up consists of a probe station, equipped with an HP 4140B meter/dc voltage source for *I-V* measurements and an HP 4192A low frequency impedance analyzer for *C-V* measurements.

This thesis came up with a plan to add optical instruments to the existing I-V and C-V measurements station, to complete an optoelectronic station so that dark current and photocurrents can be measured for optical devices. We used an optical fibre to connect the optical instruments to the probe station. The probe station is housed in a shielded enclosure and the optical instruments are outside as shown in figure 4.5 setup The shielded enclosure is used to reduce the radiation noise from the surroundings. Inside the enclosure is an optical microscope focused on the sample stage for easy selection of miniature diodes. A chopper is used for variation of for light frequencies which is housed inside the shielded enclosure, between the sample and the light. A SiC detector is used to measure the intensity of the light.. The UV monochromator can be replaced by visible range monochromator which is able to measure light

from blue to infra-red. Different light sources are available for the station: Deuterium lamp for deep UV, which has a wavelength range from 100 – 700 nm. The second monochromator is also suitable for UV measurements and is equipped with Xenon lamp for wavelengths ranging from 100 – 1100 nm. When UV light is focused on a diode, a small photocurrent is measured, which can be amplified to a voltage for determination of voltage responsivity, using an operational amplifier. The optical set-up is calibrated with a SiC detector and an AlGaN detector for UV measurements. It has been shown that the station is accurate as the commercial SiC and AlGaN detector factory specification has been reproduced at this station. All these are controlled by a LABVIEW program for dark currents, responsivity and photocurrents measurements as a function of wavelength.
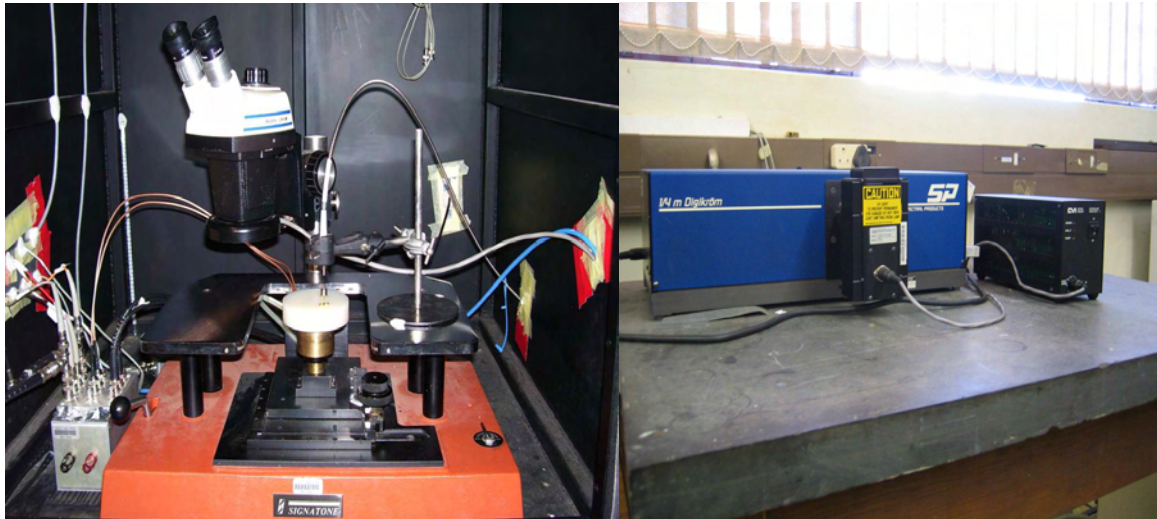

Figure 4.5: Optoelectronic device testing station: Probe stand is housed in a shielded enclosure, where measurements are done. The monochromater and deuterium lamp are connected to the station by a optical fibre.

54

REFERENCES

[1]   Davis L.E., MacDonald N. C, Palmberg P. W., Riach G. E. and Weber R. E., Handbook of Auger Electron Spectroscopy, 2nd Edition Perkin-Elmer, New York (1976) .

[2]   Chapman S. K., Working with a Scanning Electron Microscope, Lodgemark, Kent.,(1986).

[3]   Binning G and Rohrer, IBM Journal of Research and Development **30** (1986).

[4]   Schroder D. K., Semiconductor Material Device and Characterization, 2nd Edition, Interscience, New York-Wiley (1998).

[5]   Tsividid Y., Operation and Modeling of the MOS Transister, 2nd Edition, McGraw Hill, New York (1999).

[6]   Sze S. M., Physics of Semiconductor Devices, 2nd Edition, Wiley, New York (1981).